Hindawi
Geofluids
Volume 2024, Article ID 9577375, 16 pages
https://doi.org/10.1155/2024/9577375

Research Article

Effects of Internal Pressure on Urban Water Supply Pipeline Leakage-Induced Soil Subsidence Mechanisms

Jingyu Cui,[1] **Fengyin Liu**,[1] **Ruidi Chen**,[1] **Shuangshuang Wang**,[1] **Cheng Pu**,[1,2] **and Xu Zhao**[1]

[1]*Institute of Geotechnical Engineering, Xi'an University of Technology, Xi'an 710048, China*
[2]*PowerChina Northwest Engineering Corporation Limited, Xi'an 710065, China*

Correspondence should be addressed to Jingyu Cui; cuijingyu@stu.xaut.edu.cn and Fengyin Liu; fyliu211@163.com

Received 20 September 2023; Revised 27 March 2024; Accepted 30 March 2024; Published 15 April 2024

Academic Editor: Xianwei Zhang

After the rupture of pressurized water supply pipes in urban underground areas, seepage-induced ground subsidence becomes a severe geological hazard. Understanding the permeation and diffusion patterns of water in soil is crucial for deciphering the mechanisms underlying soil settlement and damage. Notably, the pressure within water supply pipes significantly influences the settlement and damage of the soil. Therefore, this study simulated experiments on soil settlement and damage caused by water seepage from a preexisting damaged pipeline under various internal pipe pressure conditions using an indoor model apparatus. The results indicate that the internal pressure of the pipe significantly influences the settlement of the soil. High-pressure seepage causes noticeable erosion in the soil, forming cavities within it. In contrast, low-pressure seepage results in water diffusing in an ellipsoidal pattern, leading to the formation of circular surface cracks. The degree of surface settlement increases with higher pipe pressure. The onset of subsidence at a specific point on the ground is not directly related to whether the moistening front within the soil has reached that point horizontally. Instead, it is associated with the moisture content below the subsidence point within the soil. The research results further illustrate the water diffusion and moisture content increase processes after water seepage from pipes with different pressures, revealing the influence of pipe pressure on the degree and form of soil settlement damage and clarifying the relationship between water diffusion and settlement in the soil.

1. Introduction

Underground water supply pipelines, as integral components of urban infrastructure, play a pivotal role in meeting daily water demands of residents and sustaining the urban environment for long-term development. However, these underground water supply pipelines may face the risk of rupturing over extended periods of use, with such rupture events potentially giving rise to a myriad of issues. A major concern is the soil settlement and ground deformation caused by the rupture of these supply pipelines. Currently, urban ground subsidence and collapse have become increasingly prevalent in China, resulting in significant economic losses and casualties [1]. Statistics compiled by Hu et al. [2] indicate that in a considerable proportion (55%) of urban ground collapse cases in China, the underlying cause can be attributed to the damage of underground pipeline system, especially in pipelines that have been in service for over 25 years, where the likelihood of leakage is notably elevated [3]. Once leakage occurs in water pipelines, it leads to erosion of the surrounding soil, ultimately resulting in ground subsidence [4–6]. With the ongoing process of urbanization, an in-depth examination of the consequences of underground water supply pipeline ruptures on soil settlement is now essential. This investigation is becoming increasingly imperative.

Many scholars and professionals have dedicated substantial efforts to address this issue in the past. Shi et al. [7] conducted a numerical analysis, utilizing a three-dimensional finite element method. Their focus was on investigating settlement induced by pipeline leakage. They emphasized that the extent of leakage is the primary determinant of settlement. Cui et al. [8] utilized the discrete element method in their

Table 1: Model experiment similarity ratio.

Physical quantity	Similarity ratio (prototype/model)	Physical quantity	Similarity ratio (prototype/model)
Length (L)	n	Stress (σ)	n
Square (S)	n^2	Strain (ε)	1
Volume (V)	n^3	Poisson's ratio (ν)	1
Displacement (D)	n	Modulus of elasticity (E_0)	n
Gravitational acceleration (g)	1	Moisture content (ω)	1
Density (ρ)	1	Permeability coefficient (k)	$n^{1/2}$
Cohesive force (c)	n	Time (t)	$n^{1/2}$
Internal friction angle (φ)	1	Liquid flow rate (Q)	n^4

study. They investigated the influence of unpressurized pipeline damage on soil settlement, considering soil particle friction coefficients and particle sizes and groundwater levels. Ibrahim and Meguid [9] conducted a detailed numerical study on the influence of pipeline crack dimensions and the height of sand fill above the pipe on erosion. Cao et al. [10], through numerical modeling, used a wetting front model to describe moisture infiltration in the soil. Qi et al. [11], using a Fluent and PFC coupled approach, investigated the variation of underground cavities following pipeline rupture, while Tang et al. [12] utilized the discrete element method to explore the erosion phenomenon caused by sewage pipelines on the surrounding soil. Zhou et al. [13] employed a CFD and DEM coupled approach to analyze the loss process of underground soil layers under the influence of water flow.

Additionally, many scholars have conducted research using physical model experiments, focusing on surface settlement and collapse patterns after sewage pipeline damage [14–17]. Ali and Choi [18] highlighted the dominant role of underground soil conditions in the mechanism of soil settlement induced by pipeline leakage, depending on the type of underground soil profile. Nazari et al. [19] conducted experiments on the flow characteristics of water in sandy soil, while Hu et al. [20] found that the moisture content of sandy soil significantly affects the morphology and magnitude of surface settlement. Karpf et al. [21] studied groundwater infiltration and sewage overflow behavior under hydraulic conditions. Cui et al. [22] conducted experiments on pressurized pipeline leakage and suggested that the soil undergoes stages of nonfluidization, cavity stabilization, and fluidization after pipeline leakage.

However, it is essential to note that the existing research has primarily focused on soil deformation and subsidence following underground pipeline rupture, with limited exploration of the effects of different pipe pressure conditions on soil settlement patterns. Different pipe pressure conditions may result in varying postpipeline rupture soil behaviors, subsequently affecting the degree and distribution of surface subsidence. This aspect has not been comprehensively investigated in previous studies.

To address this gap, in our study, we systematically conducted physical model experiments. We processed and analyzed data on moisture content and settlement collected from various points following pressurized pipeline rupture. We identified the characteristics of moisture migration and soil displacement around the damaged pipeline, revealing the relationship between pipe pressure and soil settlement patterns. This research provides robust support and references for various fields, including underground pipeline design, maintenance, urban planning, and environmental protection.

2. Experimental Device Design

2.1. Similarity Ratio Design. Model experiments must adhere to similarity criteria, where physical quantities with the same names between the prototype and the model must satisfy specific proportional relationships. These criteria primarily include geometric similarity, kinematic similarity, and dynamic similarity. The calculation of similarity ratios is achieved through the π theorem in dimensional analysis, utilizing mass (M), length (L), and time (T) as the fundamental dimensional quantities. All other physical quantities can be expressed in terms of these three fundamental dimensions. The calculated similarity ratios for this model experiment are presented in Table 1, where "n" represents the ratio of length between the prototype and the model. In this experiment, $n = 25$.

2.2. Test Model Box. The experimental model box serves as the primary experimental apparatus within the entire experimental system. It is fabricated from organic glass with a thickness of 10 mm and assembled using high-strength organic adhesive. Consequently, the box exhibits robust structural integrity and deformation resistance. The internal dimensions of the box measure $600 \times 600 \times 650$ mm. A 5 mm-thick steel plate is affixed to the top of the model box for the installation of monitoring devices. At the midpoint of both sides of the box, there are openings with a diameter of 40 mm to facilitate the subsequent laying of pipelines. On the external surface of the box, starting from the bottom, a series of calibration marks are drawn at 80 mm intervals. These marks serve the dual purpose of aiding in the observation of the thickness of each layer during the soil filling process and facilitating the monitoring of soil deformation throughout the experiment.

2.3. Hydraulic System. The hydraulic system for this experiment primarily comprises a supply tank, a storage tank, a water pump, valves, and PVC pipes. The supply tank is a

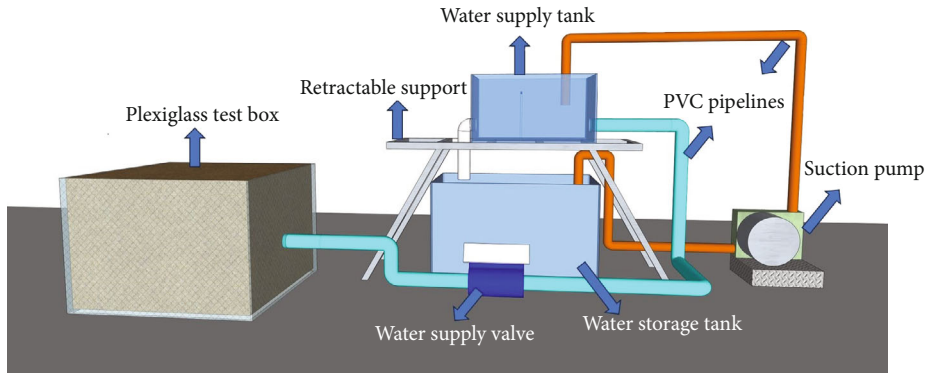

Figure 1: Experimental equipment diagram.

400 × 200 × 400 mm organic glass container, divided into two sections by a 300 mm-high organic glass overflow plate within. There are 40 mm openings on either side of the tank for connecting the supply and drainage pipes. Water from the storage tank is pumped into the right side of the supply tank, where under the influence of the overflow plate, a stable water level is maintained to ensure consistent hydraulic head throughout the system. Simultaneously, the overflowed water enters the left side of the supply tank and is directed back into the storage tank through a drainage pipe, thereby achieving water recirculation.

A 40 mm PVC pipe is passed through two openings on the model box, and at the midpoint of the PVC pipe located inside the model box, a 3.2 mm-diameter circular hole is created to simulate an actual pressurized pipeline rupture. One end of the pipeline is sealed, while the other end connects to the right-side opening of the supply tank. Additionally, a supply valve is installed to regulate the flow of water. During the experiment, the supply valve is opened. As water continuously flows into the pipe, air within the pipeline gradually exits through the circular hole, ultimately achieving a full-flow state, with water overflowing from the hole.

Figure 1 provides a schematic representation of the equipment used in this experiment.

2.4. Information Monitoring and Collection System. The data collection and monitoring system consist of three modules: the settlement monitoring module, the moisture content monitoring module, and the digital camera image monitoring module.

A set of settlement monitoring modules consists of one dial indicator, one organic glass shim, and one magnetic base, as illustrated in Figure 2. In total, there are nine sets. The dimensions of the organic glass shim are 10 × 10 mm. The dial indicator has a range of 0-50 mm with a resolution of 0.01 mm.

The moisture content monitoring module is composed of TDR soil moisture sensors and a data acquisition instrument, as illustrated in Figure 3. Seven TDR soil moisture sensors are installed at predetermined locations. During the pipeline seepage process, data on moisture content is periodically collected at regular intervals from these seven points. The data is then consolidated via a hub into a single data cable, which is subsequently input into the data acquisition instrument.

A digital camera was employed for continuous observation and image capture of the entire process of overlying soil settlement and deformation caused by pipeline rupture and seepage, as depicted in Figure 4. The continuous image capture ensured the accuracy and rigor in describing the variations in experimental phenomena.

3. Model Experiment Process

3.1. Experimental Scheme Design. In this study, we aimed to investigate the influence of varying water pressures within the pipes on soil behavior following leakage. Therefore, in the experimental design, the rupture openings of the pipes were consistently oriented upwards, and three distinct initial hydraulic heads were established to induce different pressure conditions within the pipes. The specific details of this setup are presented in Table 2.

In the model box, the experimental fill thickness is 560 mm, with the pipe buried 80 mm below the surface of the fill. The experimental soil was sourced from the extensive loess deposits found in Xi'an, a city located in the northwestern region of China. The fundamental parameters of this soil are detailed in Table 3.

3.2. Model Experiment Procedure. Based on the above experimental design, the experiment proceeded with the following steps:

(1) Inspection of water supply system sealing: connect the left side of the water supply tank to the water storage tank, the right side to the model box, and seal the pipe connections with sealing tape. Turn on the water pump and the water supply valve, and inspect all parts of the pipeline for any leakage. If there is any leakage, seal it promptly

(2) Soil filling and soil moisture sensor installation: using a layered filling method with each layer having a thickness of 80 mm, compact the soil after each layer is filled. When the filling thickness reaches the height of the preset points for the soil moisture sensors, place the sensors at the designated locations and connect the data cables to external data

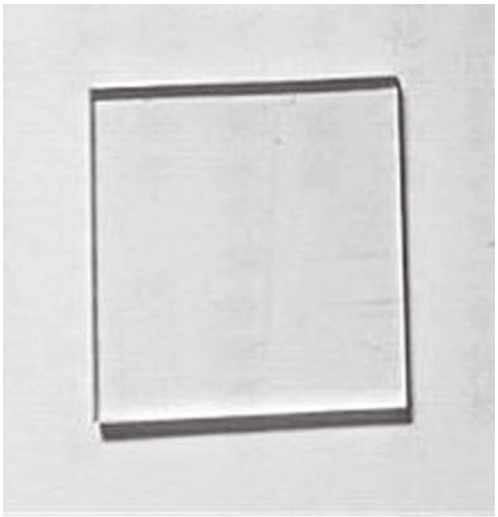

(a) Organic glass shim

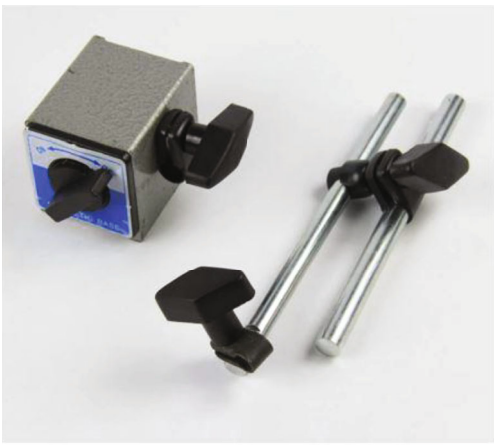

(b) Magnetic base

(c) Dial indicator

Figure 2: Settlement monitoring module.

collection equipment. Then continue filling until reaching the top layer

(3) Installation of dial indicator: after filling the soil to the top layer, place organic glass pads at the preset points. Attach the magnetic bases of the dial indicators to the steel rings on the top of the box, and then install the dial indicators on the magnetic bases. The needle of the dial indicators should be in contact with the organic glass pads, in a fully compressed state, and all dial indicator readings should be zeroed

(4) Installation of the image monitoring system: place a digital camera in a fixed position above the model box, aligning the lens with the top surface of the soil layer. Connect the power supply, use high-capacity SD storage cards, and conduct tests to ensure the proper functioning of the system

(5) Open the water supply valve: water flows out from the water supply tank. Once it reaches full-flow status, water enters the soil in the model box through the damaged section of the pipe

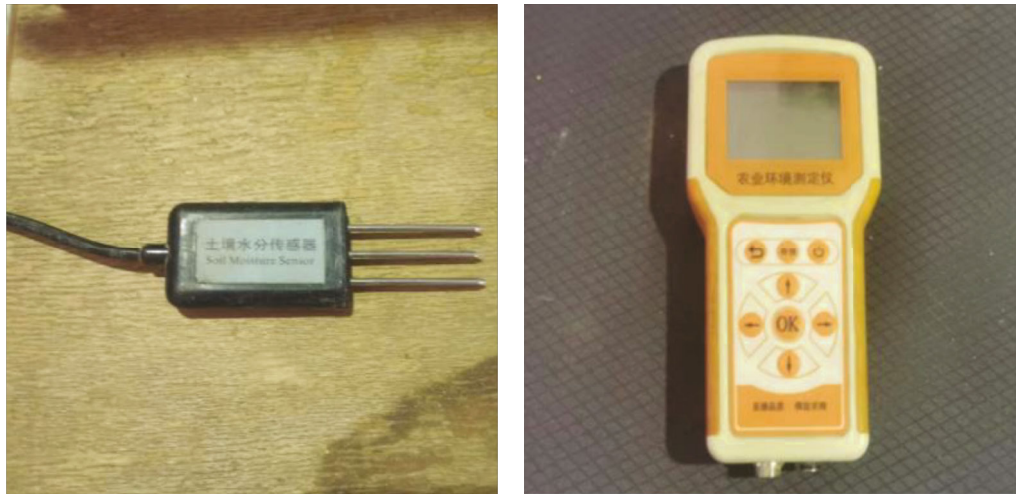

(a) TDR soil moisture sensors (b) Data acquisition instrument

Figure 3: Moisture monitoring module.

(a) Front view (b) Back view

Figure 4: Digital camera for experiments.

Table 2: Experimental scheme.

Experiment number	Initial hydraulic head
1	0.5 m
2	1.0 m
3	1.5 m

Table 3: Experimental soil parameters.

Parameter	Symbol	Numerical value
Specific gravity of soil particles	d_s	2.71
Density	ρ	1.53 g/cm^3
Moisture content	ω	4%-8%
Plastic limit	ω_P	15.78%
Liquid limit	ω_L	26.11%

(6) Data collection: after opening the water supply valve, immediately activate the soil moisture sensors and regularly record the changes in moisture content at various monitoring points near the leak location during the seepage process. Regularly manually read the settlement data at the top of the soil in the model box and use the camera to record the morphological changes of the soil surface throughout the entire process

(7) Termination criteria for the experiment: the experiment will be stopped upon the occurrence of either the breach of the surface soil layer by water flow or the manifestation of substantial soil settlement, indicative of soil failure

3.3. Model Experiment Monitoring Scheme. A total of 9 dial indicators were set up for settlement monitoring in this experiment. Through preliminary experiments, we found that the settlement of the topsoil was roughly uniformly distributed outward from the center point. Therefore, during the formal experiment, the monitoring points were arranged as shown in Figure 5, which allowed us to obtain more detailed settlement data.

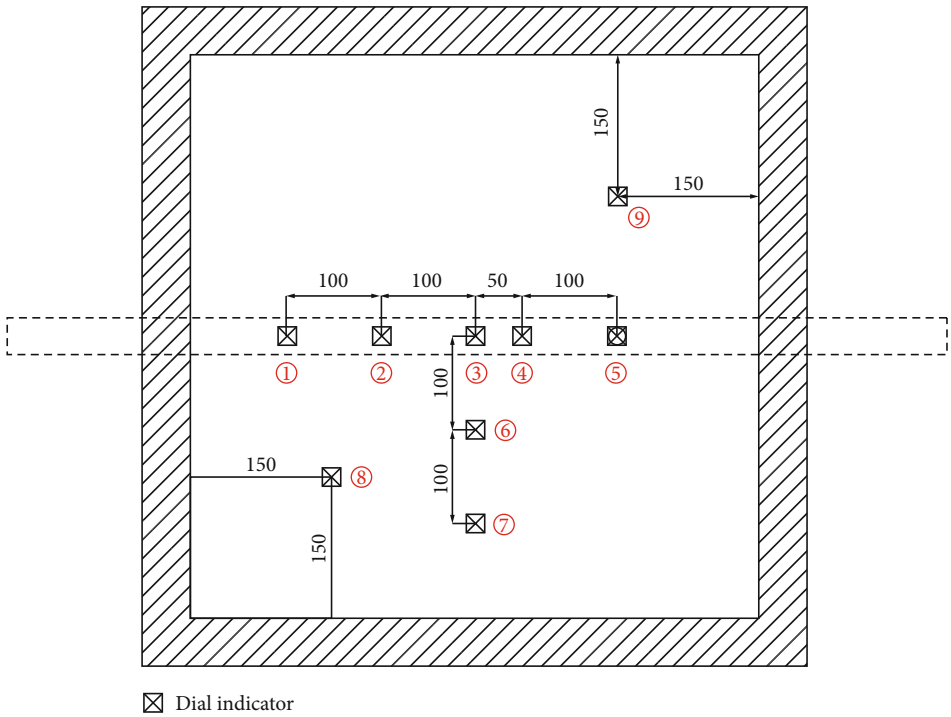

Figure 5: Diagram of dial indicator placement (top view).

Seven sets of TDR moisture sensors were deployed to monitor changes in moisture content. The variations in moisture content at different locations could reflect the extent of water diffusion in the soil. Hence, when considering the placement of moisture sensors, the horizontal distance from the leakage point and the vertical burial depth were taken into account. The final arrangement is illustrated in Figure 6.

4. Experimental Result

4.1. Experimental Phenomenon. The experiment's duration was measured from the opening of the water supply valve to the removal of the dial gauges.

Figure 7 illustrates the experimental observations when the initial hydraulic head was set at 0.5 meters. The experiment lasted for a total of 1050 minutes. At the 330-minute mark, a portion of the soil surface at the center began to show signs of being wet, indicating the arrival of the wetting front at the soil's surface. As the experiment progressed, the wetted area on the soil surface continued to expand, forming a stable circular pattern. Upon reaching 1050 minutes, the experiment was intentionally halted. Throughout this process, no significant settlement or cracking was observed.

At an initial hydraulic head of 1.0 m, some intriguing phenomena were observed during the experiment, as shown in Figure 8. The experiment lasted approximately 400 minutes. At 19 minutes, the wetting front reached the surface of the soil. At 50 minutes, cracks were observed on the soil surface, forming a circular shape with the center at the midpoint of the soil. The radius of these cracks was approximately 50 mm. At this point, the wetting front had not yet advanced to the location of these cracks.

Around 110 minutes into the experiment, a second circle of cracks appeared on the soil surface. These also had a circular shape with the center at the midpoint of the experimental soil, but with a radius of about 120 mm. The wetting front had crossed the first circle of cracks by this time but had not reached the second circle.

At the 360-minute mark, a third circle of cracks emerged. Similar to previous observations, this circle had a radius of approximately 240 mm. The wetting front had not yet reached this third circle. When the third circle of cracks appeared, the soil experienced significant settlement. The settlement exhibited a funnel-like shape, with greater deformation closer to the center point.

At an initial hydraulic head of 1.5 m, the experiment duration was further reduced to 180 minutes. By the 4-minute mark, the wetting front had already reached the surface of the soil. Subsequently, the wetting front rapidly advanced, exhibiting circular diffusion. Higher water pressure results in faster water flow, thereby intensifying the erosive impact on the soil. The movement of water mobilizes soil particles, leading to erosion on the surface of the surrounding soil. Eroded soil particles may be carried away by the leaking water, forming suspended particles or rolling and dragging in the water. This process results in a loss of soil mass. Additionally, the leaked water exerts shear forces on the soil, causing cutting and movement, which can lead to soil layer disruption and the formation of cracks. The increasing leakage of water raises the pore water pressure in the soil, reducing the soil's shear strength and rendering it more unstable. This heightened instability further elevates

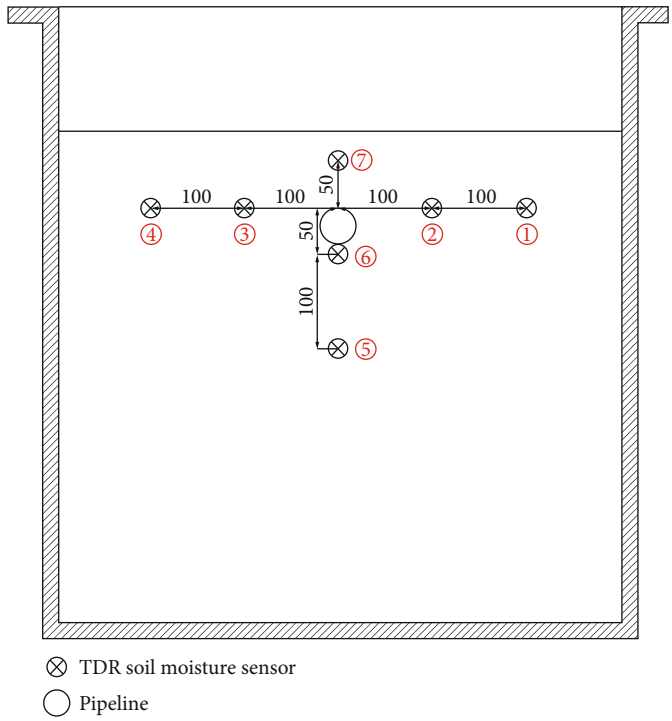

Figure 6: Diagram of TDR soil moisture sensor placement (front view).

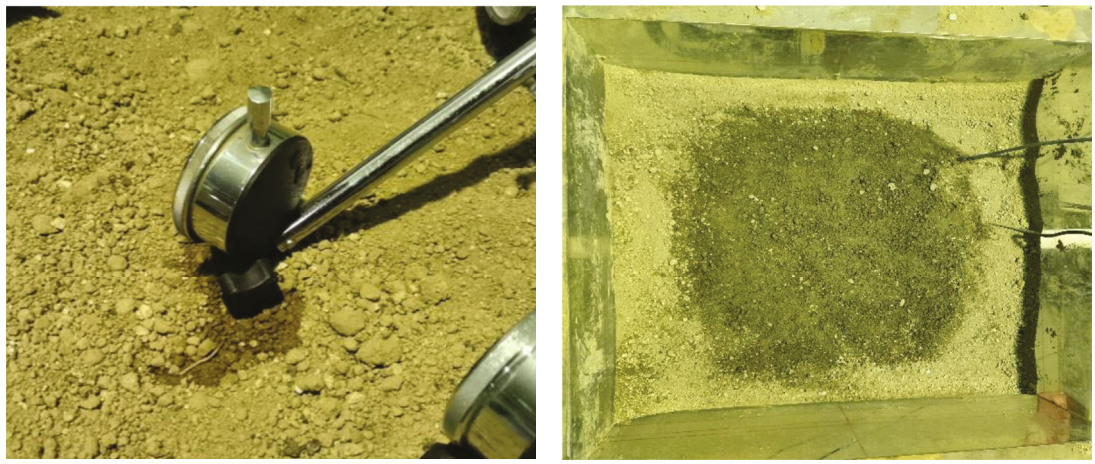

(a) 330 mins (b) 1050 mins

Figure 7: Experimental observations at 0.5 m hydraulic head.

the risk of deformation in the soil after erosion. At 120 minutes, a sinkhole with a diameter of approximately 60 mm appeared above the leakage point, leading to pressurized water jetting onto the soil surface. It rapidly spread across the entire top surface of the soil, resulting in extensive overall soil settlement. By the 180-minute mark, due to the presence of a buried pipeline in the central portion of the soil layer, there was resistance to the subsidence of the soil. Consequently, the soil above the pipeline experienced less settlement compared to the soil near the edges of the model box. Additionally, a tensile crack that traversed the experimental soil formed along the pipeline's path. The destructive phenomena are illustrated in Figure 9.

4.2. Variations in Moisture Content around the Leakage Orifice. Based on the arrangement of the TDR moisture sensors mentioned above, the moisture content of the soil around the leakage orifice was monitored, and the curves showing the changes in soil moisture content at different initial hydraulic heads over time were obtained. As shown in Figure 10(a), when the initial hydraulic head was 0.5 m, points 2#, 3#, and 7# exhibited earlier changes in moisture content, followed by point 6#, and points 1#, 4#, and 5# showed the latest changes in moisture content. This indicates a direct relationship between the response time of moisture content at different points after the pipeline leakage and the distance between that point and the leakage

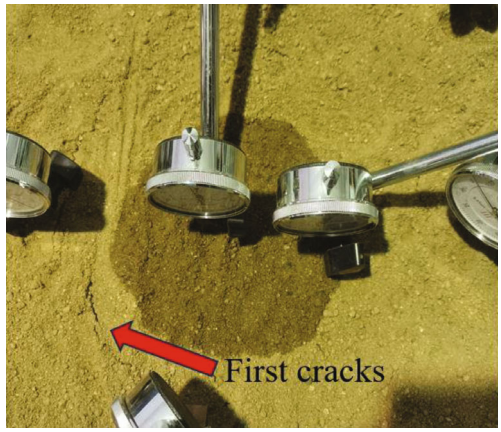

(a) 50 mins

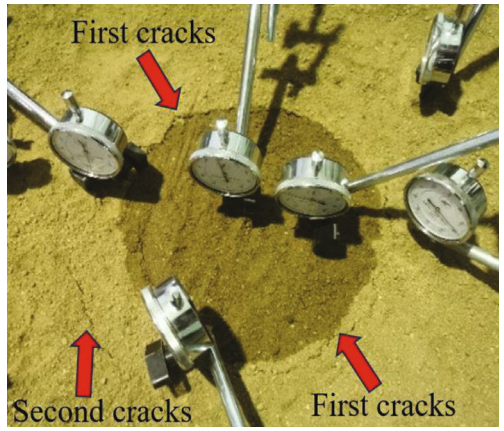

(b) 110 mins

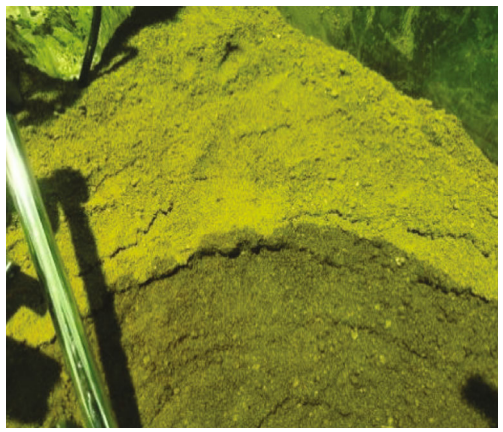

(c) 400 mins

Figure 8: Experimental observations at 1.0 m hydraulic head.

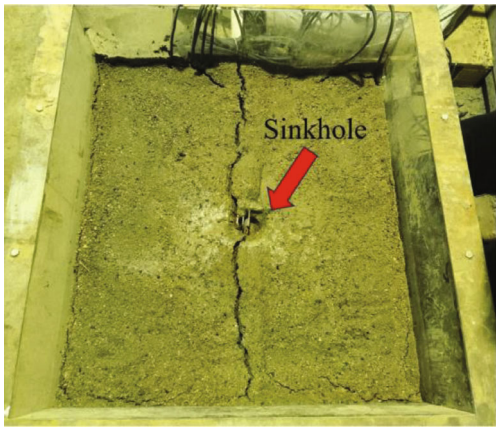

(a) Erosion hole damage

(b) Measuring hole diameter

Figure 9: Experimental observations at 1.5 m hydraulic head.

orifice. In the final stage of the experiment, the moisture content at each point tended to stabilize, with little variation, all around 16% to 20%. It is inferred that there was no dominant preferential flow channel within the soil throughout the experiment.

At an initial hydraulic head of 1.0 m, the order in which moisture content started to change at different points was consistent with the 0.5 m hydraulic head results, but three changes occurred, as explained in conjunction with Figure 10(b): (1) Point 7# located above the leakage orifice

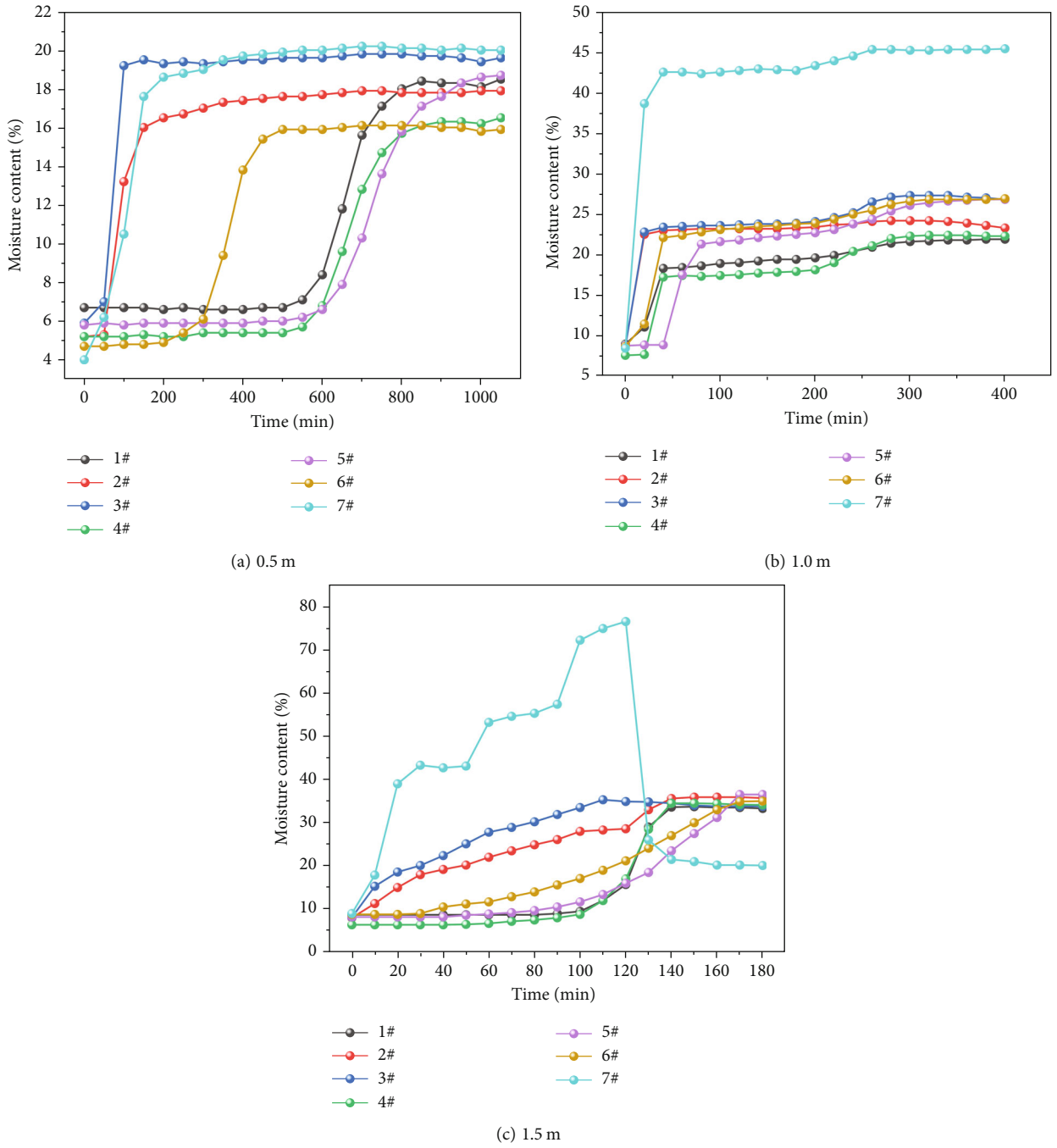

Figure 10: The variations in moisture content at different hydraulic heads.

exhibited a rapid increase in moisture content, reaching 40% within 20 minutes and stabilizing at 45%, which was much higher than the 20% in the previous experiment. (2) The time interval between the start of moisture content changes at different points, which was significantly longer at a 0.5 m hydraulic head, noticeably shortened at a 1.0 m hydraulic head, with the wetting front reaching all seven measurement points within 70 minutes. (3) In the later stages of the experiment, the moisture content of point 7# at 45% was significantly higher than the 20%-25% of the other six points.

When the hydraulic head was 1.5 m, the moisture content variations at different measurement points are shown in Figure 10(c). In comparison with the results at a 1.0 m hydraulic head, this experiment revealed two significant differences: (1) Point 7# continued to exhibit rapid increases in moisture content, but not continuously; instead, it increased in stages. The moisture content values once again exceeded the previous experiment, reaching around 80% at 120 minutes and subsequently decreasing to stabilize at around 20%. (2) Although the initial hydraulic head increased, the time for the remaining six points to exhibit changes in

moisture content did not decrease compared to the 1.0 m hydraulic head condition. Furthermore, the increase in moisture content was more gradual, and at the end of the experiment, it stabilized at around 30%.

4.3. The Correspondence between Leakage Rate and Diffusion. In this study, the experimental setup is incapable of monitoring real-time leakage rates at the pipeline breach. Instead, we calculated the average leakage rates for each experiment based on the time taken and total water-permeated data at the end of the experiment. The average leakage rates for experiments with water heads of 5 kPa, 10 kPa, and 15 kPa were 0.038 L/min, 0.1125 L/min, and 0.34 L/min, respectively. Given the difficulty in capturing the internal moisture diffusion range within the soil, we represent the diffusion range using the circular radius of the wetted area on the soil surface. The relationship between leakage rates and diffusion range is illustrated in Figure 11.

From the graph, it is evident that in the initial stages of experiments with higher leakage rates, the horizontal diffusion speed of water on the soil surface is faster. A higher leakage rate results in a larger diffusion range over the same time period. In the experiment with an initial water head of 1.5 m, at 120 minutes into the experiment, holes appeared on the soil surface, leading to a substantial outflow of water through these holes. The leaked water rapidly propagated and diffused along the soil surface, causing a quick increase in the diffusion range. In the other two experiments where similar holes did not form, the experiment with an initial water head of 1.0 m showed a slower increase in diffusion range over time. This is because as water permeates and diffuses within the soil, it takes on an ellipsoidal shape, and with each increment in the semiaxis of the ellipsoid, the volume of the ellipsoid increases exponentially. Therefore, more water is required, leading to a longer duration, particularly under stable leakage rates. In the experiment with an initial water head of 0.5 m, where the leakage rate at the breach is smaller, water predominantly infiltrates horizontally and downwards within the soil, resulting in a delayed appearance of wetness on the soil surface. The experimental apparatus in this study does not allow for the internal visualization of the soil during experiments. Therefore, using the radius of the wetted soil surface to represent the diffusion range of water has certain limitations.

4.4. The Variation Patterns of Surface Settlement in Soil. Figure 12 illustrates the settlement results from experiments conducted under three different hydraulic head conditions. It is evident that higher hydraulic heads result in more pronounced settlements, and the differences in values are substantial. For water heads of 0.5 m and 1.0 m, the magnitude of settlement at different measurement points is generally related to their distance from the central point, similar to the relationship observed in changes in moisture content. Points closer to the center exhibit larger settlements, while those farther away experience smaller settlements. However, this pattern is not as distinct as the relationship observed in moisture content changes. For instance, as shown in Figure 12(b), points 5# and 6# are equidistant from the center, but their final

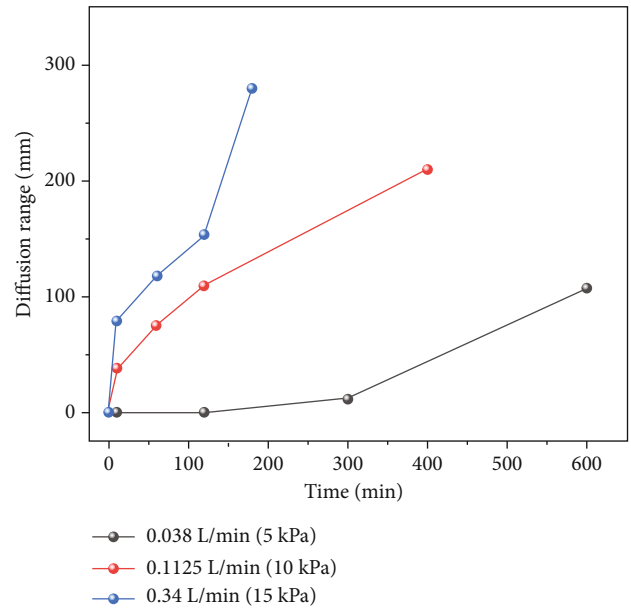

Figure 11: Leakage rate and diffusion range correlation curve.

settlement values differ, with 5# consistently showing less settlement compared to points 8# and 9#.

Under a hydraulic head of 1.5 m, in the middle to early stages of the experiment, the settlement at point 4# consistently exceeded that at the central point 3#. At 120 minutes, significant erosion by water flow resulted in the formation of a noticeable cavity on the soil surface. Subsequently, a large volume of water overflowed onto the surface throughout the model box. Starting from this moment, the entire soil mass within the model box accelerated its settlement. Consequently, tension cracks formed along the pipeline direction, causing the dial needles of the 1#, 2#, 3#, 4#, and 5# dial indicators, which were oriented along the pipeline, to suspend in midair, making further measurements impossible. The remaining four points exhibited settlements exceeding 30 mm, with the maximum approaching 50 mm.

5. Discussion

Guo et al. [14] suggest that the hydraulic head determines the geometric shape of erosion cavities and establishes the relationship between soil erosion rate and cavity diameter. This is based on the condition of having holes at the bottom of the experimental box, which facilitates significant soil erosion. In practical engineering, the direction of soil erosion may not necessarily be stable directly beneath the pipeline. The underground soil can be considered a closed environment; therefore, the bottom of the model box in this study adopts a closed structure. Cui et al. [22] demonstrated that the hydraulic pressure on eroded soil is not solely determined by the initial hydraulic head; the size of the pipeline breach also plays a decisive role. This finding is crucial for our study, as it led us to set a uniform breach size while only varying the initial hydraulic head. This approach allows for a

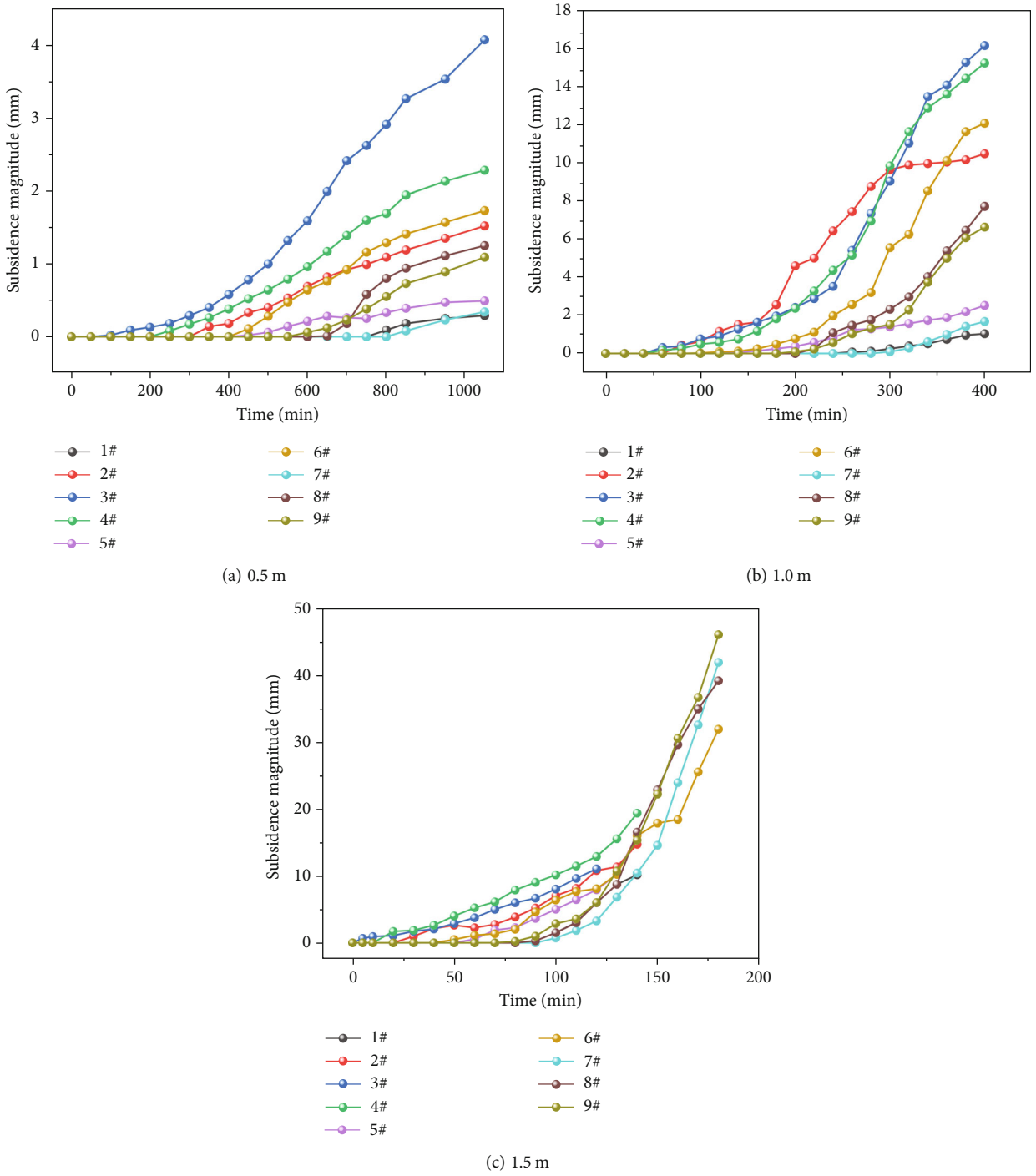

Figure 12: The variation in settlement at different hydraulic heads.

better exploration of the relationship between internal pipeline pressure and infiltration-induced failure.

In this study, at a hydraulic head of 1.5 m, the experiments resulted in the direct formation of erosion holes on the soil surface, leading to a substantial overflow of water that filled the model box. This, in turn, caused significant overall settlement of the soil mass. However, in the two sets of experiments where erosion holes did not form on the soil surface, the settlement results were consistent with what has been presented in literature [16, 17]. In these cases, the settlement exhibited a conical distribution pattern, with the maximum settlement occurring directly above the pipeline leakage point, as shown in Figure 13.

Nevertheless, this study also revealed some phenomena that differed from the results reported in literature [16, 17]. In the investigations conducted in these two prior studies, higher water pressures led to the formation of relatively large-sized cavities within the internal soil mass of the model box, subsequently resulting in settlement and subsidence. However, in this study, under hydraulic head conditions of

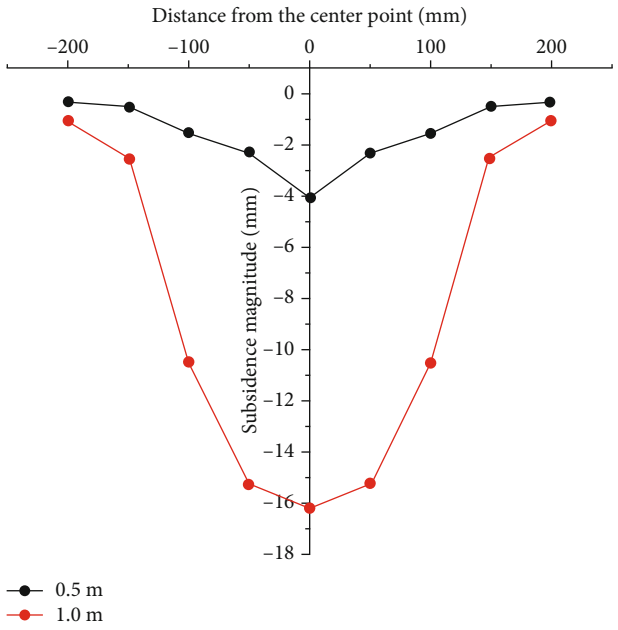

Figure 13: Experimental settlement curve.

0.5 m and 1.0 m, no significant cavities were observed during the postexperiment inspection of the internal soil mass. This suggests that, even without the formation of cavities, pipeline leakage can still induce ground settlement. Interestingly, during the settlement process under a 1.0 m hydraulic head, regular concentric cracks were observed on the soil surface, a phenomenon not observed at the 0.5 m hydraulic head.

The experimental methodology in this study features two notable improvements compared to previous research. Firstly, in terms of the water supply system, the implementation of an overflow plate within the water supply tank ensures a stable hydraulic head. Furthermore, varying the height of the water tank facilitates the investigation of different hydraulic head levels. This exploration helps assess their impact on the experiments. Importantly, the entire system has been designed to facilitate the recycling of water, thereby minimizing resource wastage.

Secondly, in this experiment, the pipeline leakage point was positioned at the center of the model box, as opposed to the sidewall of the box. While this approach does not allow for the direct observation of the water flow's configuration when it spills over, it effectively eliminates the boundary effects associated with rigid sidewalls. Consequently, this adjustment provides a more realistic representation of the actual soil-water interactions.

5.1. The Impact of Moisture Diffusion on Settlement. The diffusion of moisture within the soil plays a significant role in shaping the patterns of settlement. Therefore, it is crucial to understand the diffusion patterns of moisture within the soil. By conducting function fittings on the moisture content data collected from seven different measurement points in the experiment, we were able to derive seven equations. Plotting these equations reveals the time at which moisture content began to change at each measurement point. Taking the experiment with a 1.0 m water head as an example, the results are shown in Table 4.

Table 4: Initiation times of moisture content changes at different measurement points under 1.0 m hydraulic head.

Measurement point	Initiation time of moisture content alteration
1#	24 mins
2#	2 mins
3#	2 mins
4#	21 mins
5#	mins
6#	5 mins
7#	1 min

When studying the diffusion of moisture, the concept of the wetting front is of paramount importance. It indicates the interface to which moisture has advanced at a given moment. When the moisture content at a measurement point begins to change, it signifies that the wetting front has progressed to that location. Since the distances between various measurement points and the center point are known, the advancement speed of the wetting front in a single direction can be determined.

To analyze the curves depicting the horizontal, upward vertical, and downward vertical progression distances of the wetting front over time, power functions were employed for fitting. The results are expressed as $f(x_1)$, $f(x_2)$, and $f(x_3)$, respectively. The outcomes are as follows:

$$\begin{aligned} f(x_1) &= 40.9971x_1^{0.2864}, \\ f(x_2) &= 30.0932x_2^{0.3155}, \\ f(x_3) &= 29.3723x_3^{0.2842}. \end{aligned} \tag{1}$$

In the equation above, x represents time.

Hence, based on the aforementioned formula, the diffusion changes of the wetting front under the 1.0 m hydraulic head condition can be represented in Figure 14. Results obtained through fitting calculations indicate that following the pipeline leakage, the moisture diffusion pattern takes the form of an incomplete ellipsoid. After the experiment's conclusion, the dry soil was excavated, leaving only the moist soil. Through observation, it was evident that the moisture diffusion pattern closely matched the computed results, as depicted in Figure 15.

Upon substituting time into the aforementioned formula, the advancement profile of the wetting front at any given moment can be computed. Based on experimental data, it can be observed that at a hydraulic head of 1.0 m, settlement was detected at monitoring point 6# after 100 minutes of the experiment, and at monitoring point 7# after 300 minutes. By substituting these two time values into the formula mentioned above, two wetting front advancement boundaries can be determined, as illustrated in Figure 16. From the graph, it is evident that at the moments of

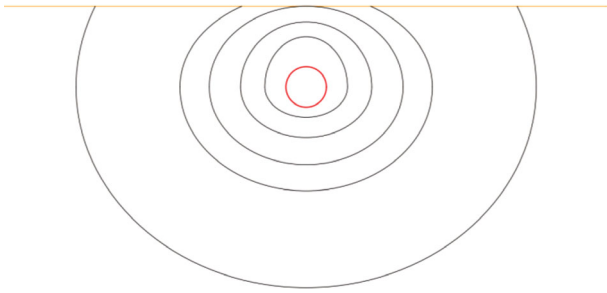

Figure 14: Diagram of wetting front dispersion changes.

Figure 15: The moisture dispersion morphology after the experiment.

settlement at 6# and 7# points, the horizontal advancement distance of the wetting front had already exceeded that of the corresponding monitoring points. This leads to the inference that soil settlement is not directly correlated with the arrival of the wetting front but rather influenced primarily by the magnitude of moisture content.

The research findings of Hu et al. [20] also demonstrate that soil moisture content significantly influences both the morphology and magnitude of surface subsidence. Moreover, when the moisture content is below a certain threshold, an increase in moisture content notably facilitates a reduction in the magnitude of surface subsidence. The experimental results with a hydraulic head of 0.5 m precisely reflect this phenomenon. In the case of relatively dry soil, after a certain period of low-pressure infiltration and diffusion, there is a gradual increase in soil moisture content. Consequently, the time required to reach the threshold is prolonged, thereby delaying the magnitude and rate of soil subsidence. This is also the reason for the significantly lower final subsidence observed compared to a hydraulic head of 1.0 m.

The study by Karoui et al. [15] demonstrates that the direction of water flow in the soil influences the development direction of soil voids, ultimately determining the location of ground subsidence. The results of this experiment validate Karoui's findings and further confirm that even in the absence of cavity in the soil, the location of ground subsidence remains closely associated with the direction of water flow in the soil.

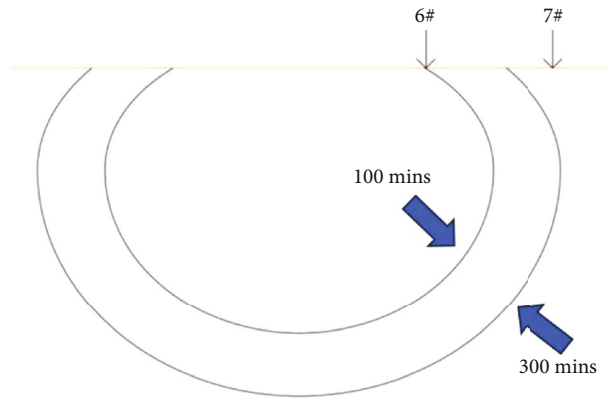

Figure 16: The advancement interface of the wetting front at the time of settlement occurrence.

5.2. The Causes of Circular Crack Formation. Figure 17 illustrates the relationship between the rate of moisture content increase at measurement points and time at 0.5 m and 1.0 m head. From the data in the figure, it can be observed that at the lower hydraulic head, the rate of moisture content increase at various measurement points is significantly slower compared to the higher hydraulic head. Moreover, at a hydraulic head of 1.0 m, all 7 measurement points experienced rapid moisture content increase in the early stages of the experiment. This is the fundamental reason for the different experimental outcomes observed in the two sets of experiments.

Water infiltrates the soil under higher pressure, causing the rapid advancement of the wetting front within the soil. Within a certain region, the moisture content rises rapidly, resulting in significant differences in saturation levels between different interfaces within the soil. The side with higher moisture content experiences a rapid increase in self-weight, making it more susceptible to sliding against adjacent, drier soil. This, in turn, leads to the formation of intermittent sliding cracks.

The increase in self-weight simultaneously compacts the soil below, reducing the pore volume of the underlying soil. Additionally, the abundance of water can dissolve soluble salts in the soil, further decreasing the volume of the high-moisture region, resulting in soil settlement. This phenomenon can be hypothesized as follows, as illustrated in Figure 18: Moisture leaks from the damaged point and diffuses in an ellipsoidal shape. Therefore, settlement primarily occurs within the ellipsoid. As the ellipsoid settles, the protruding parts of the soil above it act like small, rigid cantilever beams. With an increase in the downward movement of the ellipsoid, these protruding cantilever beams become longer until their rigidity cannot withstand the force of gravity, leading to fracture. This process repeats step by step as the wet ellipsoid expands, giving rise to the observed phenomenon in the experiment.

Currently, research on such issues through model experiments mainly focuses on soil properties, hydraulic

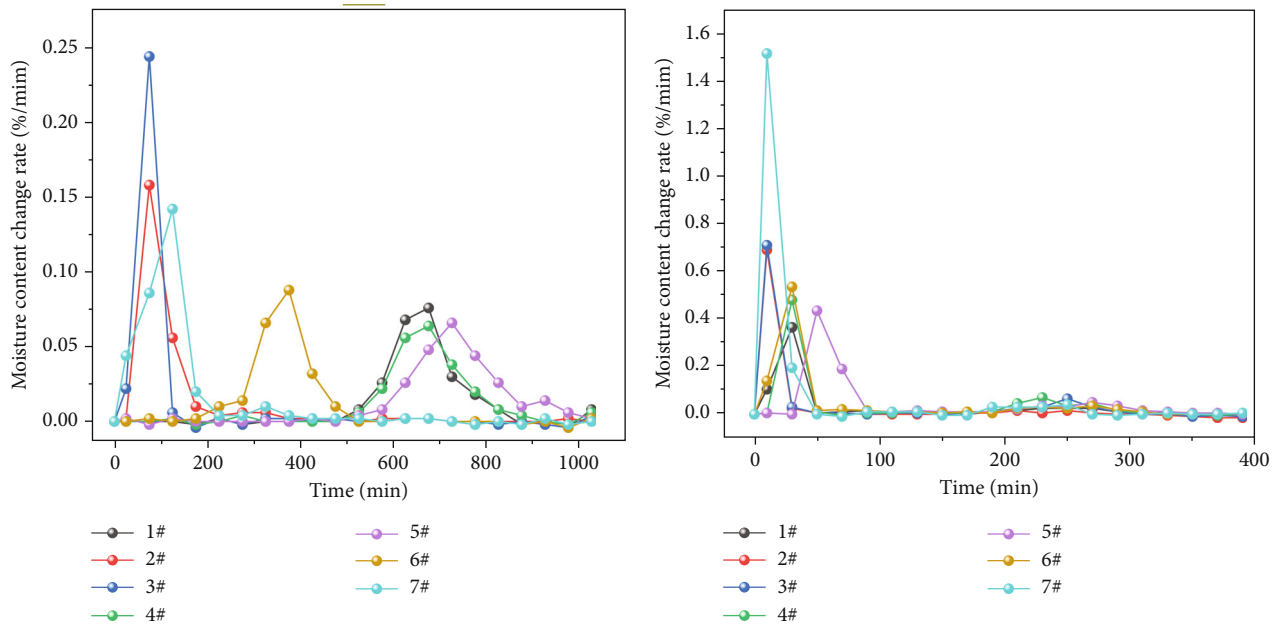

(a) 0.5 m (b) 1.0 m

Figure 17: The rate of change in moisture content.

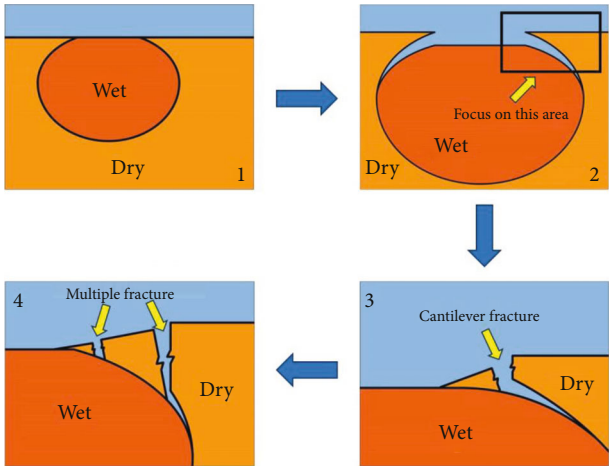

Figure 18: The mechanism of circular crack formation.

head inside the pipeline, and the size of the pipeline breach. By tracking the movement of soil particles and the evolution of soil cavity, researchers aim to explain the mechanisms behind collapse and subsidence. However, the initial condition for soil subsidence or collapse is the infiltration of water into the supply pipe. Therefore, understanding the infiltration and diffusion patterns of water after leaking from the breach under different pressures is crucial. This directly leads to different failure modes in the soil, not necessarily all due to the formation of cavity. The findings of this study can further enrich our understanding of issues related to the infiltration-induced failure of soil around pipelines.

However, due to limitations in the experimental setup, real-time data on moisture content variations cannot be obtained. Only data within certain time intervals can be measured, which may result in the time point of moisture content change occurring between two successive measurements. The timing of moisture content change is crucial as it is related to the advancement rate of the wetting front in the soil, ultimately affecting our prediction of the range of water infiltration. This also leads to a lack of information on the variation of moisture content curve slope over time. The change in slope signifies the arrival of the wetting front, and when the slope no longer changes, it indicates soil saturation. Between these two time points, the slope variation can better reflect which direction is the predominant flow pathway, further enhancing our understanding of water diffusion trends in the soil. The absence of this information may, to some extent, interfere with our judgment.

In the future, research on related issues can benefit from the utilization of more advanced measuring instruments for real-time data recording, thereby avoiding the need for interpolation. Additionally, modeling and computational analysis of relevant problems using finite element software can provide visual representation of results through visualization and postprocessing capabilities. This allows for intuitive presentation of results and facilitates extraction of useful information by capturing data on key points.

6. Conclusion

This paper employs a water circulation supply system, a soil model box, and predamaged pipelines to simulate the phenomenon of subterranean soil settlement damage induced by leakage in pressurized pipelines with preexisting flaws. By manipulating the water pressure within the pipes, the study monitors variations in moisture content and settlement patterns at different measurement points under

various water pressure conditions. Surface observations are also conducted to investigate the impact of water diffusion on ground settlement damage after pipeline leakage under different water pressure scenarios. The experimental results are distinctly clear, and the summarized conclusions are as follows:

(1) Pipe pressure primarily influences the erosive kinetic energy of the outflowing water at the existing damaged site. When the pipe pressure is substantial, the impact of the water flow is pronounced, resulting in the soil's susceptibility to the formation of erosive cavities, leading to collapse. In cases where the pipe pressure is insufficient to create cavities through erosion, higher pipe pressure contributes to a more rapid diffusion of water in the soil and an accelerated increase in soil moisture content

(2) By observing experimental phenomena and deducing from experimental data, the diffusion of moisture within the soil exhibits an ellipsoidal pattern

(3) In the absence of surface erosive cavities or collapse, the ground settlement trough exhibits a conical shape, with the maximum settlement occurring directly above the leakage point in the pipeline. The greater the water pressure within the pipe, the larger the maximum settlement observed

(4) At a water head of 1.0 m, the formation of circular cracks in the surface-dry region is attributed to the settlement of the ellipsoidal moist soil within the soil mass. This settlement leads to the dry soil at the top edge adopting a cantilever beam shape, which subsequently undergoes brittle failure under the influence of gravity

Finally, regarding the issue of ground subsidence caused by leakage from damaged water supply pipelines, and based on the findings of this study, five recommendations are proposed for practical engineering:

(1) For urban planners, during the design and planning phase of urban pipeline systems, considerations should be made regarding the layout and drainage design of the pipelines. It is advisable to avoid placing pipelines in areas sensitive to ground subsidence as much as possible. Where conditions permit, pipelines should be placed within an underground integrated pipe gallery to prevent direct contact between pipelines and soil, thereby reducing the potential damage caused by pipeline ruptures. Additionally, it is essential to establish a comprehensive maintenance system. Based on factors such as pipeline materials, service life, and surrounding environment, the maintenance cycle and scope of the pipeline system should be clearly defined. Detailed inspection standards and procedures should be developed, encompassing exterior inspections, pressure testing, leak detection, and corrosion inspections, among others. Inspection procedures should outline steps, tools, equipment, and safety measures involved

(2) For engineers, the design of underground pipelines should consider selecting materials with sufficient strength and corrosion resistance, such as steel and polyethylene. Based on the environment in which the pipeline is located and the anticipated water pressure, the thickness and structure of the pipeline should be designed to ensure that it can withstand the expected pressure and hydraulic impact. Depending on the actual requirements and anticipated water pressure, it is important to control the pressure and flow rate of the pipeline reasonably. Through devices such as pipeline valves and regulators, control of the water flow should be exercised to avoid excessively high or low pipeline pressures

(3) Conduct more detailed geological exploration and investigation of the soil around pipelines. Comprehensive understanding of the engineering geological characteristics of underground soil can provide a more accurate basis for design work and reduce the risk of soil subsidence

(4) To establish a comprehensive monitoring system, real-time data monitoring of pipeline operation should be conducted using devices such as pipeline pressure sensors and flow meters. Monitoring points should cover critical locations along the pipeline, such as the starting point, endpoint, and bends. Regarding monitoring devices, after installation, calibration should be performed regularly to ensure the reliability and accuracy of the equipment. Simultaneously, an alarm mechanism should be established, setting thresholds for monitoring data. Once the monitored data exceeds the predetermined thresholds, immediate alarm notifications should be issued to facilitate timely measures to address potential risks

(5) From the perspective of engineering materials, further research and development of new pipeline materials with higher corrosion resistance and better erosion resistance should be pursued. This would help improve the lifespan of pipelines and mitigate the impact of pipeline damage on the surrounding soil

These measures will undoubtedly have a positive impact on public safety in urban areas as well as the sustainability of society and the environment.

Data Availability

The data used to support the findings of this study are included within the article.

Conflicts of Interest

The authors declare that they have no conflicts of interest.

Acknowledgments

This study was funded by the National Natural Science Foundation of China (nos. 51679198 and 12072260) and the State Key Laboratory of Eco-hydraulics in the Northwest Arid Region of China (QNZX-2019-07).

References

[1] X. W. Wang and Y. S. Xu, "Investigation on the phenomena and influence factors of urban ground collapse in China," *Natural Hazards*, vol. 113, no. 1, pp. 1–33, 2022.

[2] Y. H. Hu, Y. C. Bai, and H. J. Xu, "Analysis of reasons for urban road collapse and prevention and control countermeasures in recent decade of China," *Highway*, vol. 61, no. 9, pp. 130–135, 2016.

[3] R. Kuwano, T. Horii, H. Kohashi, and K. Yamauchi, "Defects of sewer pipes causing cave-in's in the road," in *In Proceedings of the 5th International Symposium on New Technologies for Urban Safety of Mega Cities in Asia*, pp. 16-17, Phuket, Thailand, 2006.

[4] M. Balkaya, I. D. Moore, and A. Sağlamer, "Study of nonuniform bedding support because of erosion under cast iron water distribution pipes," *Journal of Geotechnical and Geoenvironmental Engineering*, vol. 138, no. 10, pp. 1247–1256, 2012.

[5] M. Toshifumi, K. Naoko, and O. Jun, "Image analysis of soil failure on defective underground pipe due to cyclic water supply and drainage using X-ray CT," *Frontiers of Structural and Civil Engineering*, vol. 6, no. 2, pp. 85–100, 2012.

[6] J. E. Van Zyl, M. O. Alsaydalani, C. R. Clayton, T. Bird, and A. Dennis, "Soil fluidisation outside leaks in water distribution pipes—preliminary observations," *Water Management*, vol. 166, no. 10, pp. 546–555, 2013.

[7] X. Shi, Y. Cao, C. Rong, G. An, H. Wang, and L. Cui, "Influence of pipeline leakage on the ground settlement around the tunnel during shield tunnelling," *Sustainability*, vol. 14, no. 24, p. 16802, 2022.

[8] J. Y. Cui, F. Y. Liu, Y. W. Geng, C. Pu, and M. Miao, "Numerical simulation of ground subsidence factors resulting from unpressurized pipeline rupture below the water table," *Applied Sciences*, vol. 13, no. 17, p. 9536, 2023.

[9] A. Ibrahim and M. A. Meguid, "CFD-DEM simulation of sand erosion into defective gravity pipes under constant groundwater table," *Tunnelling and Underground Space Technology*, vol. 131, article 104823, 2023.

[10] Y. Cao, M. Xu, P. Ni, and G. Mei, "Physical and numerical modelling of infiltration from drainage holes for perforated storm sewer," *Acta Geotechnica*, vol. 17, no. 2, pp. 527–543, 2022.

[11] G. Qi, Z. Wang, Y. Chen et al., "Analysis of instability mechanism and induced cause of urban pavement in Xining City, China," *Advances in Materials Science and Engineering*, vol. 2022, Article ID 3365402, 12 pages, 2022.

[12] Y. Tang, D. H. Chan, and D. Z. Zhu, "A coupled discrete element model for the simulation of soil and water flow through an orifice," *International Journal for Numerical and Analytical Methods in Geomechanics*, vol. 41, no. 14, pp. 1477–1493, 2017.

[13] H. T. Zhou, C. Q. Liu, G. H. Wang, K. Kang, and Y. H. Liu, "Study on drilling ground collapse induced by groundwater flow and prevention based on a coupled CFD-DEM method," *KSCE Journal of Civil Engineering*, vol. 26, no. 5, pp. 2112–2125, 2022.

[14] S. Guo, Y. Shao, T. Zhang, D. Z. Zhu, and Y. Zhang, "Physical modeling on sand erosion around defective sewer pipes under the influence of groundwater," *Journal of Hydraulic Engineering*, vol. 139, no. 12, pp. 1247–1257, 2013.

[15] T. Karoui, S. Y. Jeong, Y. H. Jeong, and D. S. Kim, "Experimental study of ground subsidence mechanism caused by sewer pipe cracks," *Applied Sciences*, vol. 8, no. 5, p. 679, 2018.

[16] F. Tan, W. Tan, F. Yan, X. Qi, Q. Li, and Z. Hong, "Model test analysis of subsurface cavity and ground collapse due to broken pipe leakage," *Applied Sciences*, vol. 12, no. 24, p. 13017, 2022.

[17] S. Indiketiya, P. Jegatheesan, and P. Rajeev, "Evaluation of defective sewer pipe–induced internal erosion and associated ground deformation using laboratory model test," *Canadian Geotechnical Journal*, vol. 54, no. 8, pp. 1184–1195, 2017.

[18] H. Ali and J. H. Choi, "Risk prediction of sinkhole occurrence for different subsurface soil profiles due to leakage from underground sewer and water pipelines," *Sustainability*, vol. 12, no. 1, p. 310, 2020.

[19] S. Nazari, R. Gholami, and S. Mirassi, "Laboratory evaluation of scour rate and energy dissipation in gabion stepped weirs with considering the effect of discharge and tail water depth," *Journal of Applied Science and Agriculture*, vol. 9, no. 4, pp. 1424–1439, 2014.

[20] X. Hu, C. He, Z. Peng, and W. Yang, "Analysis of ground settlement induced by earth pressure balance shield tunneling in sandy soils with different water contents," *Sustainable Cities and Society*, vol. 45, pp. 296–306, 2019.

[21] C. Karpf, S. Hoeft, C. Scheffer, L. Fuchs, and P. Krebs, "Groundwater infiltration, surface water inflow and sewerage exfiltration considering hydrodynamic conditions in sewer systems," *Water Science and Technology*, vol. 63, no. 9, pp. 1841–1848, 2011.

[22] X. L. Cui, G. L. Tao, and J. Li, "Experiment and numerical simulation on seepage failure of sand caused by leakage of underground water pipe," *In IOP Conference Series: Earth and Environmental Science*, vol. 153, no. 3, article 032033, 2018.